


Modeling navigation by weaver ants in an unfamiliar, featureless environmentTheerawee Thiwatwanikul  and Panyaphong Paisanpan *School of Physics, Suranaree University of Technology, Nakhon Ratchasima 30000, Thailand*

Sukrit Suksombat

*School of Sports Science, Suranaree University of Technology, Nakhon Ratchasima 30000, Thailand*M. F. Smith *School of Physics, Suranaree University of Technology, Nakhon Ratchasima 30000, Thailand
and NANOTEC-SUT Center of Excellence on Advanced Functional Nanomaterials, Suranaree University of Technology,
Nakhon Ratchasima 30000, Thailand*(Received 29 September 2019; revised manuscript received 22 March 2020; accepted 13 April 2020;
published 14 May 2020)

The motion of individual weaver ants from *Oecophylla smaragdina* was tracked within a small arena to study the algorithm that these ants use for navigation. The arena, a floor tile, was either clean or partly covered by a mild chemical repellent. Statistical properties of the observed motion of the ant can be described by a model that is analogous to the Langevin theory of the motion of Brownian particles. With each time step, the velocity of the ant changes by a random vector with a robust probability distribution. When the average ant encounters the chemical repellent it responds, like a particle seeing a potential energy barrier, by initially slowing before recovering towards its equilibrium state of motion. The model accounts for most qualitative properties of motion with a small number of parameters.

DOI: [10.1103/PhysRevE.101.052404](https://doi.org/10.1103/PhysRevE.101.052404)**I. INTRODUCTION**

Weaver ants include *Oecophylla longinoda*, native to Africa, and *Oecophylla smaragdina*, from tropical Asia and Australia. They are remarkable for making large-scale cooperative efforts [1,2]. Thousands of individuals work together to weave nests in trees by folding and gluing broad leaves, or to form bridges from the bodies of the ants themselves. This requires communication over a range of length scales [3,4]. The mechanisms of communication employed by weaver ants, using pheromones, gestures, and direct contact, are indeed sophisticated and have attracted the longtime interest of biologists [5–8]. They also make them an attractive subject for the physics of collective phenomena in complex systems [9–12]. The effect of communication on ant motion, in particular, is a topic of interest [8,13–15].

In this paper we take a quantitative approach to a simple aspect of the behavior of an individual from *Oecophylla smaragdina*, its motion within a small arena. The arena is a floor tile that is normally featureless except for its square boundary but can be modified by coating part of the tile with a chemical repellent. We track the position of each ant in the arena versus time, and based on the results develop a model of individual ant movement that is analogous to the Langevin theory of Brownian motion. The algorithm that the ant uses to navigate is represented by the parameters of this model. While we hope to later investigate how communication between different ants can affect the algorithm, this paper is concerned only with navigation by an individual ant.

There is an apparent similarity between the erratic motion of a foraging ant and that of a Brownian particle. In biophys-

ical modeling, a Brownian motion picture is often taken as a basis for more sophisticated theories of navigation by ants and many other animals [16–28]. Much current research along these lines is motivated by the idea of using ant motion as an example of general collective motion of communicating individuals: as macroscopic versions of bacterial processes relevant to medicine, as models for human crowds or for designs of swarming robots, as a few examples [29–33].

A Brownian particle, like a grain of pollen in water, undergoes dispersive motion because of its collisions with surrounding water molecules. Einstein explained the motion using a statistical description of these collisions, and Langevin further developed this theory a few years later [34]. In Langevin's theory of Brownian motion, the particle is subject to random impulses, forces applied over a short duration that have random direction and zero time average, as well as deterministic forces like a drag force and an interaction with external fields. Since the dominant forces on the ant are reaction forces of the ground on its moving body parts, all parameters in a Langevin model of ant motion can be interpreted as features of the navigation algorithm employed by the ant.

We apply Langevin's theory to the motion of individual weaver ants, and find that random and deterministic components of the forces can be resolved. The probability distribution of random impulses is robust and characterized by a single parameter. The deterministic response to the chemical repellent can be modelled by an external field or 'potential energy' that indicates the desirability of a given position. The theory explains most statistical properties of the data including the counterintuitive observation that ants, which

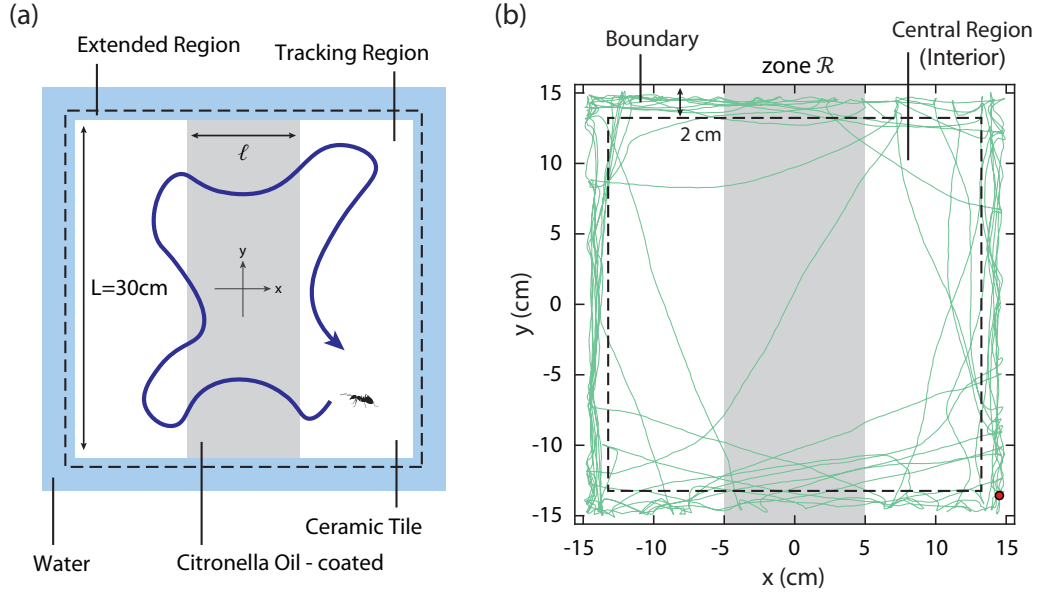


FIG. 1. (a) The experimental setup for observing ant movement with a camera mounted above the arena, a square floor tile of length $L = 30\text{ cm}$. The position of an ant can be detected slightly beyond the boundary of the arena, in the extended region. (b) The dark (green) path is an actual ant trajectory in a clean arena. The gray shaded band, centered along x and of width ℓ will be called zone \mathcal{R} . It has no significance for the clean arena but indicates where citronella oil is to be coated. The dashed line distinguishes a strip along the boundary, with $d = 2\text{ cm}$, from the rest of the arena (i.e., from the “interior”).

avoid the repellent and spend most of their time in the clean regions, remain continuously within a region contaminated by repellent for a longer duration than in a clean region of the same size. The mathematical simplicity of the model, which allows a full characterization of navigation with a small number of parameters, suggests that it is an appropriate starting point for further quantitative studies.

II. EXPERIMENTAL PROCEDURE

Individual major-workers from *Oecophylla smaragdina*, belonging to one of several colonies, were captured from wooded areas on the campus of Suranaree University of Technology, Nakhon Ratchasima, Thailand. Their motion was studied in two similar configurations (see Fig. 1). In both cases, the ant was free to move on the surface of a square plate, ceramic floor tile, with a side length $L = 30\text{ cm}$ and a thickness of 0.6 cm . The plate was in a larger bowl containing water, not deep enough to reach the plate surface, so ants at the plate edge encountered a water barrier that they rarely attempted to cross. We used more than a dozen tiles, nearly indistinguishable from one another, and changed the tile with each trial. After being used, a tile was washed in dishwashing soap and water and left to dry. It was eventually re-used as we cycled through tiles, but never on the same day.

In the first configuration, the plate is clean and the square arena is approximately homogeneous. In the second, a central rectangular band was coated evenly with 1% w/w citronella oil, a natural repellent that is aversive but nonlethal to ants [35,36]. This band, of width ℓ , is referred to as zone \mathcal{R} in Fig. 1. Values $\ell = 2.5$ and 10 cm were used in different experiments. We will use x, y position coordinates with the

origin at the plate center. The arena is defined by $-L/2 \leq x \leq L/2$ and $-L/2 \leq y \leq L/2$ or $|x| < 15\text{ cm}$, $|y| < 15\text{ cm}$. The repellent, when present, is coated evenly over the region $|x| < \ell/2$.

For each trial, a single ant, having been captured using a clean plastic container, was transferred into the arena by inverting this container. Within a few seconds after each ant was introduced, we started recording its motion with a video camera and did so for time $T = 300\text{ s}$ before similarly removing it from the arena. There was no evident change in behavior seen over the 300 s. A typical ant continued moving throughout the trial.

The high-speed camera was fixed to a tripod and positioned directly above the arena. In-house image processing scripts coded in MATLAB extracted the position of the ant from each frame. (The details about the image processing are included in Appendix A.) Two-dimensional spatial coordinates $\mathbf{r}(t) = (x[t], y[t])$ were obtained at discrete time steps $t = j\Delta t$ with $j = 0, 1, 2, \dots, 4500$ and $\Delta t = 1/15\text{ s}$. A sample trajectory is shown in Fig. 1(b). Because of the ant's finite body size, its position is occasionally found in the extended region, 0.5 cm beyond the arena.

A probability distribution, i.e., a normalized histogram for position $\Pi(x, y)$, is plotted in Fig. 2. We counted the number of times that the position $x[t], y[t]$ of the ant in any trial landed in each square bin, $\Delta x = 0.3\text{ mm}$ in length. Dividing by the total number of events, this gives a probability density $\Pi(x, y, t)$ for finding an ant near $\mathbf{r} = (x, y)$ at time t . Averaging over time gives the normalized histogram $\Pi(x, y) = (1/T) \int dt \Pi(x, y, t)$ that tells us the fraction of time that the average ant spends near a given position. The quantity $\Pi(x, y)$ has units $1/\text{cm}^2$ and its integral over the entire arena is equal to 1.

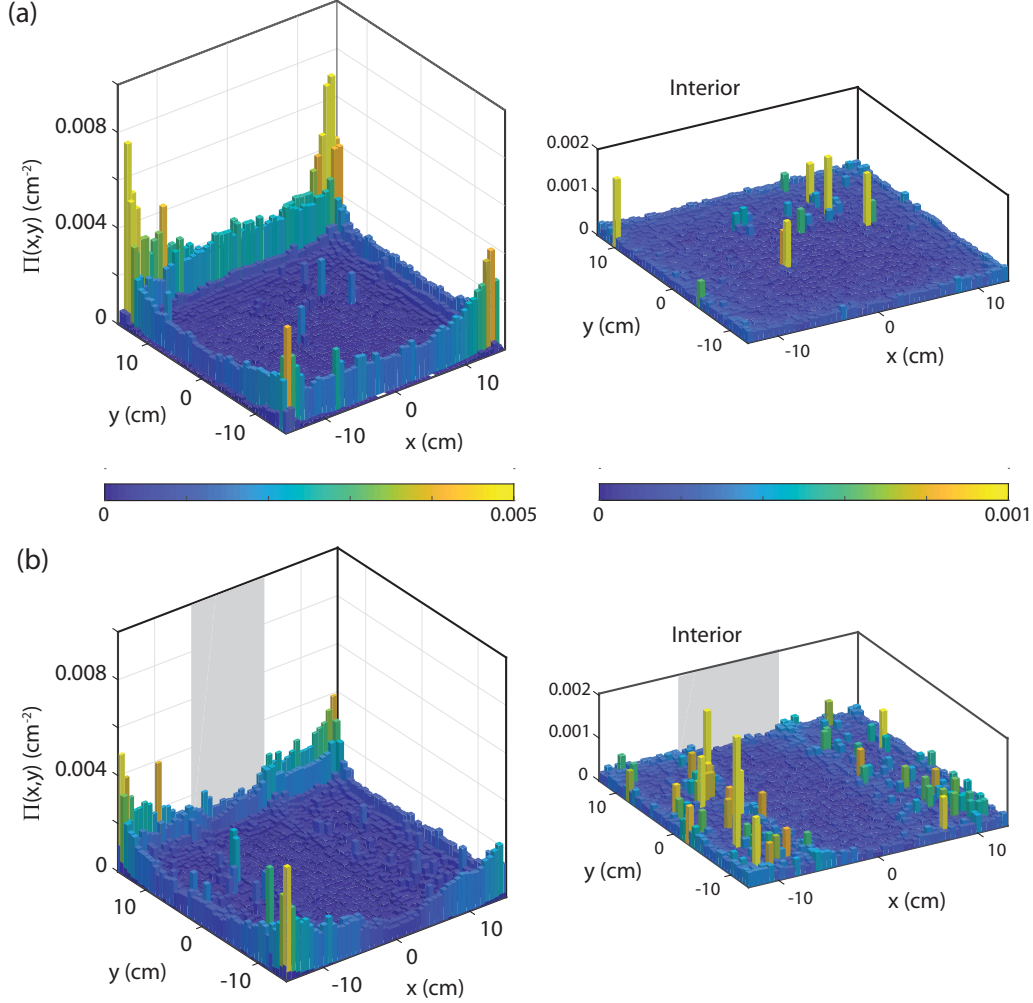


FIG. 2. Normalized position histograms. The x, y axes indicate position and the vertical axis is $\Pi(x, y)$, the probability density for ants within the arena. To make three-dimensional (3D) plots easier to see, histogram bars are colored according to height, so the color scale duplicates the vertical axis. Left plots: (a) Data for 59 ants in the clean arena. (b) Data for 68 ants with the repellent, citronella oil, painted in zone \mathcal{R} . Right plots: Same as left but with data restricted to the arena interior, $|x|, |y| > L/2 - d$.

From Figs. 1(b) and 2 we see that ants are often near the boundary. This tendency dominates the position distribution. They have a slightly reduced probability to be found in zone \mathcal{R} with and without the repellent is 0.20 ± 0.01 and 0.23 ± 0.01 , respectively. This modest difference, being comparable to the uncertainty in the measurement, is barely perceptible in the overall distribution (left in Fig. 2) but does appear in a plot of the distribution over the arena interior (right in Fig. 2). We noticed large qualitative differences between individuals: certain ants avoid the repellent while others seemed indifferent to it.

To model and analyze motion, we exploit the square symmetry of the arena that results in approximate square symmetry in the data. That is, each tile appeared square so we arbitrarily orientated it with edges along the x and y axes. While an ant might perceive asymmetry in an individual tile that we cannot, the x and y directions should be symmetry-equivalent in an average over many tiles. This symmetry is limited to the tile itself: the position of the tripod, room lighting, etc., did not maintain it. So, if the ant navigates

using the local properties of the tile then we expect data for a clean arena to respect square symmetry on average. If the ant gives significant consideration to sensory cues originating from beyond the tile then we should see a difference between the x and y directions. Deviations from square symmetry are seen below but are a small effect.

III. THEORETICAL MODEL

Most statistical properties of the data can be captured by a simple theoretical model, in which the ant is treated as a particle undergoing Brownian motion. More details of the model are given in Appendix B. In this section, we use a broad overview of the data to motivate it and then discuss nontrivial model predictions. As seen in Fig. 2, ants spend a large fraction of their time near the arena boundary. The unnatural boundary is peculiar to our experiment so ant behavior near the boundary is of no general interest. For this reason, we focus on properties of the data in which the ant-boundary interaction does not play a dominant role.

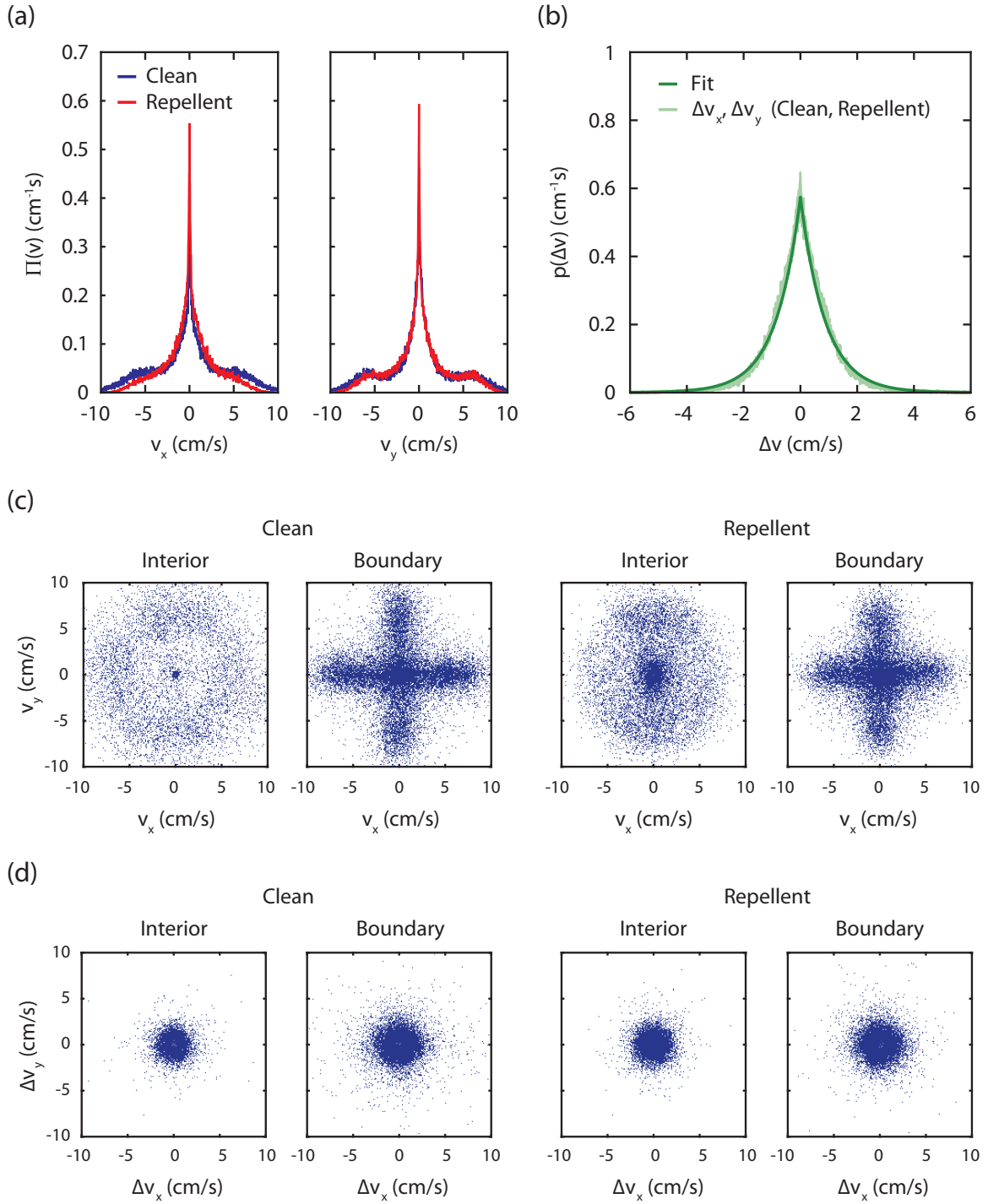


FIG. 3. Ant velocity and change in velocity derived from the position data of Fig. 2. (a) Normalized histograms of ant velocity v_x (left) and v_y (right) for ants in a “clean” arena (blue) and in an arena with a “repellent” present in zone \mathcal{R} (red). The probability density labeled $\Pi(v)$ refers to $Pi(v_x)$ and $\Pi(v_y)$ for respective components. (b) The light-green curve shows normalized histograms for velocity changes: Δv_x , Δv_y , with and without repellent present drawn on top of each other. The dark green curve is the one-parameter fit of Eq. (2) with $m = 1$ to the probability density $p(\Delta v)$. (For noncolor plots, the dark green curve is smoother.) (c) Maps in velocity space, one point per ant per time step. They show data for the arena “interior” and “boundary” strip without and with repellent. (d) Maps in $(\Delta v_x, \Delta v_y)$ space.

A. Velocity and velocity-change distributions

The position $\mathbf{r}_i(t) = (x_i[t], y_i[t])$ of $i = 1, 2, \dots, 59$ ant individuals was measured in the clean arena, where time t increases in steps $\Delta t = (1/15)$ s from $t = 0$ to $t = 300$ s.

From this, we derive the velocity $\mathbf{v}_i(t) = \Delta \mathbf{r}_i / \Delta t$ with $\Delta \mathbf{r}_i = \mathbf{r}_i(t + \Delta t) - \mathbf{r}_i(t)$ and the change in velocity $\Delta \mathbf{v}_i(t) = \mathbf{v}_i(t + \Delta t) - \mathbf{v}_i(t)$ at each time step.

Figure 3 presents normalized histograms and maps in phase space. We define a probability distribution of velocity,

$\Pi(v_x, v_y, t)$, the probability of finding an ant with a velocity in a bin centered on v_x, v_y at time t . Averaging this over time yields $\Pi(v_x, v_y) = (1/T) \int dt \Pi(v_x, v_y, t)$. To obtain a one-dimensional histogram we can further integrate $\Pi(v_x, v_y)$ over all v_y . The resulting distribution, giving the average probability of finding an ant with a given v_x , is shown in Fig. 3(a). Curves are shown for both v_x and v_y for the “clean” arena and for an arena with the “repellent” citronella oil present for $|x| < \ell/2 = 5$ cm.

The velocity distribution is peaked at zero with shoulder features seen near velocities of 5–6 cm/s. A typical ant does not remain still for long but, since it passes through zero velocity each time it turns around, it has a high probability to have a velocity near zero. The shoulders are broad plateaus that contain a local maximum. There is an increased probability for an ant to have a velocity within the shoulder region. The shoulders are notably missing from the v_x distribution when citronella oil is present, which we will discuss again in Sec. IV C.

Figure 3(c) shows maps in (v_x, v_y) space, with one data point per time step per ant. These data were divided according to position: data for the “interior” have positions at least $d = 2$ cm away from the boundary, while data for the “boundary” were obtained within the strip of width d . The latter looks like a plus sign because ants move along edges. While it appears to obey square symmetry, the velocity distribution is strongly affected by the ant-boundary interaction.

We show histograms and phase space maps for the change in velocity $(\Delta v_x, \Delta v_y)$ in Figs. 3(b) and 3(d). The phase space maps in Fig. 3(d) appear isotropic. The distributions in Fig. 3(b) are symmetric, peaked at zero, and do not change noticeably when repellent is added. Apparently they are not dominated by ant-boundary effects since results are similar near the boundary and within the arena interior. The simple distribution of Δv_x motivates the application of Langevin’s theory: velocity changes can be attributed to random local impulses with a robust probability distribution.

B. Ant as a Brownian particle

An analogy to the Langevin theory of Brownian motion is used to model ant movement. The model ant experiences a total force $\mathbf{F}(t)$ that results in a change of velocity $\Delta \mathbf{v} = \mathbf{F}(t)\Delta t = (F_x(t)\Delta t, F_y(t)\Delta t)$ with each time step. The velocity is taken to obey Newton’s second law, for unit mass, which is

$$\frac{\Delta \mathbf{v}}{\Delta t} \approx \frac{d\mathbf{v}}{dt} = \mathbf{F}(t) = \eta(t)/\Delta t - \frac{\mathbf{v}}{\tau} + \mathbf{E}. \quad (1)$$

The interaction of a Brownian particle with molecules in the ambient fluid results in a random impulse $\eta(t)$, with zero time average, and a linear drag force with time constant τ . We include these terms in the equation of motion for the ant: the random impulse, because its precise motion is unpredictable, and the drag force to keep the model stable.

The field $\mathbf{E} = \mathbf{E}(x, y)$ in Eq. (1) accounts for an ant’s interaction with any spatially dependent feature, such as the arena edges or the chemical repellent. An appropriate model for the field must be chosen in each case. Since ants stop at the arena boundary, the boundary field can be described

by a short-range repulsive force with a damping effect (like the normal force of a crash pad). For the chemical repellent, we define a potential energy $V(x, y)$ related to the field by $\mathbf{E} = -\nabla V$ that indicates the desirability of a given position (the higher the potential the less desirable the position) and assign a positive potential to a position coated with repellent.

While Δv_x is proportional to the total force F_x , the normalized histogram of Δv_x in Fig. 3(b) should be approximately proportional to the probability distribution for the random impulse η_x alone. This is mainly because the magnitude of η_x is larger than the impulse due to the other forces in Eq. (1). The effect of the latter is further reduced by square symmetry. A histogram bin contains position and velocity components with both signs and the field is odd in x and y while the drag force is odd in v_x and v_y . In this way we can approximately disentangle the random and deterministic forces.

The histogram for either component of force, assumed equal to the probability distribution $p(\eta)$ for $\eta = \eta_x$ or $\eta = \eta_y$, is fit to the following generalized Gaussian:

$$p(\eta) = N \exp\left(\frac{-|\eta|^m}{(c_m \sigma)^m}\right), \quad (2)$$

with a dimensionless number $c_m = \Gamma^{1/2}(1/m)\Gamma^{-1/2}(3/m)$ and normalization factor $N^{-1} = c_m \sigma \Gamma(1 + 1/m)$ where $\Gamma(z)$ is the Gamma function. Since $p(\eta)$ is an even function, the mean $\{\eta\} = 0$ while the mean square is

$$\{\eta^2\} = \int_{-\infty}^{\infty} d\eta \eta^2 p(\eta) = \sigma^2. \quad (3)$$

So σ is the standard deviation of the model distribution. A similar goodness of fit is found (see Appendix A) over a range of values for σ and m , so we fix $m = 1$, leaving σ as the only parameter. A Gaussian, with $m = 2$, does not give a good fit for any σ . The fits shown in Fig. 3 use $m = 1$ and the best-fit values of $\sigma_x^2 = 1.51 \pm 0.01 \text{ cm}^2 \text{ s}^{-2}$ and $\sigma_y^2 = 1.41 \pm 0.01 \text{ cm}^2 \text{ s}^{-2}$. [We denote by σ_x and σ_y the value of σ that gives the best fit to the $p(\Delta v_x)$ distribution and $p(\Delta v_y)$ distribution, respectively.]

In the model $\eta(t)$ is independently drawn at each time step. This ignores any correlations between the random impulses at nearby times: an assumption, tested later, that is made here for simplicity. Also, with η_x and η_y drawn independently and the field vector \mathbf{E} assumed to respect square symmetry, the Cartesian components of Eq. (1) are independent.

C. Measurable model properties

Using the general picture given above, we can calculate specific properties of model ant behavior that may be compared to measurements. Below we sketch derivations of each model result and describe how the corresponding property can be extracted from data. We are primarily concerned with properties that are insensitive to the details of the ant-boundary interaction.

1. Time-dependent squared velocity in the interior of a clean arena

First, we consider the mean-squared velocity of an ensemble of model ants. Write one component of the velocity as $v_x(t + \Delta t) = v_x(t) + \Delta v_x(t)$ and square this expression to

obtain

$$v_x^2(t + \Delta t) - v_x^2(t) = 2v_x(t)\Delta v_x(t) + [\Delta v_x(t)]^2. \quad (4)$$

The left side is Δt multiplied by $d(v_x^2[t])/dt$ while on the right side we use $\Delta v_x = \Delta t(dv_x/dt)$ and substitute Eq. (1). We take an ensemble average, denoted by curly brackets, by averaging over many identical ants with the same position and velocity at time t . Different members of the ensemble experience different random impulses so $\{\eta_x\} = 0$. Random impulses affect $\{v_x^2\}$ via the term proportional to $\{\eta_x^2\} = \sigma^2$ that appears on the right side of Eq. (4). The ensemble average of Eq. (4) is

$$\frac{d}{dt}\{v_x^2\} = \frac{\sigma^2}{\Delta t} - 2\frac{\{v_x^2\}}{\tau} + 2\{v_x E_x\}, \quad (5)$$

where we dropped $(\Delta t)^2$ terms.

Equation (5) can be easily solved in the case of an infinite clean arena with $E_x = 0$ everywhere. The result is

$$\{v_x^2(t)\} = v_\infty^2 + [\{v_x^2(0)\} - v_\infty^2]e^{-2t/\tau}, \quad (6)$$

where $v_\infty^2 = \sigma^2\tau/(2\Delta t)$. At large times the system is in an equilibrium state with a root-mean-square velocity component equal to v_∞ . In a large, finite arena, a sizable fraction of ants will have root-mean-square velocities close to this equilibrium value. If we attribute the shoulder features in the velocity distribution to the fraction of the ensemble that has achieved equilibrium, then we get an estimate $v_\infty \approx 5.3$ cm/s (from the peak of the shoulder feature in Fig. 3 for the clean arena). A model ant disturbed by the field will wander into a clean region and forget the disturbance in time τ and over a distance $v_\infty\tau$.

In a finite arena, we must model the ant-boundary interaction. The simplest plausible interaction is to have an ant stop abruptly at an arena edge, with v_x going to zero at $x = -L/2$ while v_y is unaffected. This crude approximation is not adequate to describe ant motion near the boundary, but can be used to study the motion of ants in the interior of the arena that have recently come from the boundary. We define the interior by $|x|, |y| < L/2 - d$, which excludes a boundary strip of width $d = 2$ cm. Then Eq. (5) is used to calculate model ensemble averages of the squared velocity in the arena interior.

These squared velocities can be compared to corresponding measured values. We compile data segments with an ant entering the interior at time t_1 and exiting at t_2 . Subtracting t_1 from t we have an experimental ensemble of ants entering the interior at $t = 0$. It is a large ensemble because each ant will enter and exit the interior region many times.

2. Position-dependent squared velocity with and without repellent

The model also predicts that an ensemble-averaged squared velocity depends on position. Ants that move away from a disturbance approach the equilibrium state of an infinite arena, so $\{v_x^2\}$ and $\{v_y^2\}$ approach v_∞^2 . For the clean arena, $\{v_x^2\}$ is small near $x = \pm L/2$ and approaches v_∞^2 deep in the interior. With repellent present, ants receive a negative (positive) impulse as they enter (leave) zone \mathcal{R} . Away from these disturbances at the borders of zone \mathcal{R} , the squared velocity again approaches v_∞^2 . To obtain the experimental

position-dependent squared velocity, we take the full data set and arrange it in order of increasing x before taking a running average of v_x^2 and v_y^2 .

3. Field and potential

The field \mathbf{E} in Eq. (1) comes from the arena boundary and chemical repellent. The boundary field, which keeps ants in the arena, is strong, short ranged, and directed inwards. The potential associated with the repellent $V(x)$ is a square barrier, with height V_0 and width ℓ . The resulting field has an x component $E_x = -V_0\delta(x + \ell) + V_0\delta(x - \ell)$ and no y component. The ant that moves into zone \mathcal{R} has to overcome a potential barrier and any ant with velocity less than $v_{\min} = \sqrt{2V_0}$ cannot enter.

Experimental values for the field $E_x(x)$ and potential $V(x)$ can be obtained in the following way. When we arrange the data in order of increasing x , break it into bins of width Δx , and take a running average of Δv_x , we obtain Δv_x as a function of x . The values of (t, y, v_x, v_y) vary within each bin and the bin average of η_x is zero. The drag force is not required by symmetry to have an average of zero but it turns out to be negligible. This means that every term on the right side of Eq. (1) can be ignored except the field $E_x(x)$. Thus, the running average of Δv_x gives $E_x(x)\Delta t$, effectively measuring the field. The integral $V(x) = -\int dx E(x)$ with $V(x) = 0$ outside zone \mathcal{R} gives the potential.

4. Crossing probability and residence time

A model ant, having entered zone \mathcal{R} , has a probability P_C to proceed through it, rather than turn back to the zone from which it came. The average time that it resides in zone \mathcal{R} before leaving to either side is T_R . In Appendix B, we calculate P_C and T_R for the model, assuming the ensemble arriving at the border is in equilibrium, as functions of the potential V_0 . For a clean arena we can take $V_0 = 0$. Both quantities can be measured by finding all instances where an ant enters zone \mathcal{R} at time t_1 and then determining the time t_2 when it exits that zone and noting to which side.

IV. RESULTS AND DISCUSSION

A. Distribution of random impulses

The most basic quantity to measure and analyze is the probability distribution of velocity changes Δv_x and Δv_y . In the Langevin model, Eq. (2) describes the distribution of random local impulses η_x that dominate the distribution $p(\Delta v_x)$ of velocity changes. We can fit the measured $p(\Delta v_x)$ to Eq. (2) with a single parameter σ . If $p(\Delta v_x)$ was determined entirely by random impulses then the value of σ would be the same for all positions and times. But the field \mathbf{E} has some influence on $p(\Delta v_x)$ and consequently on the value of the parameter σ that gives its best fit. So, apparent changes in σ reflect deterministic effects as well.

Equation (2) was used in fits to the distributions $p(\Delta v_x)$, $p(\Delta v_y)$ for several subsets of the data, with results shown in Fig. 4 and Table I. The subsets are “overall” (data for all ants at all times and positions in the clean arena), “early,” and “late” (all positions in the clean arena at time $0 < t < 30$ s and $270 < t < 300$ s, respectively), “interior” (all times in the

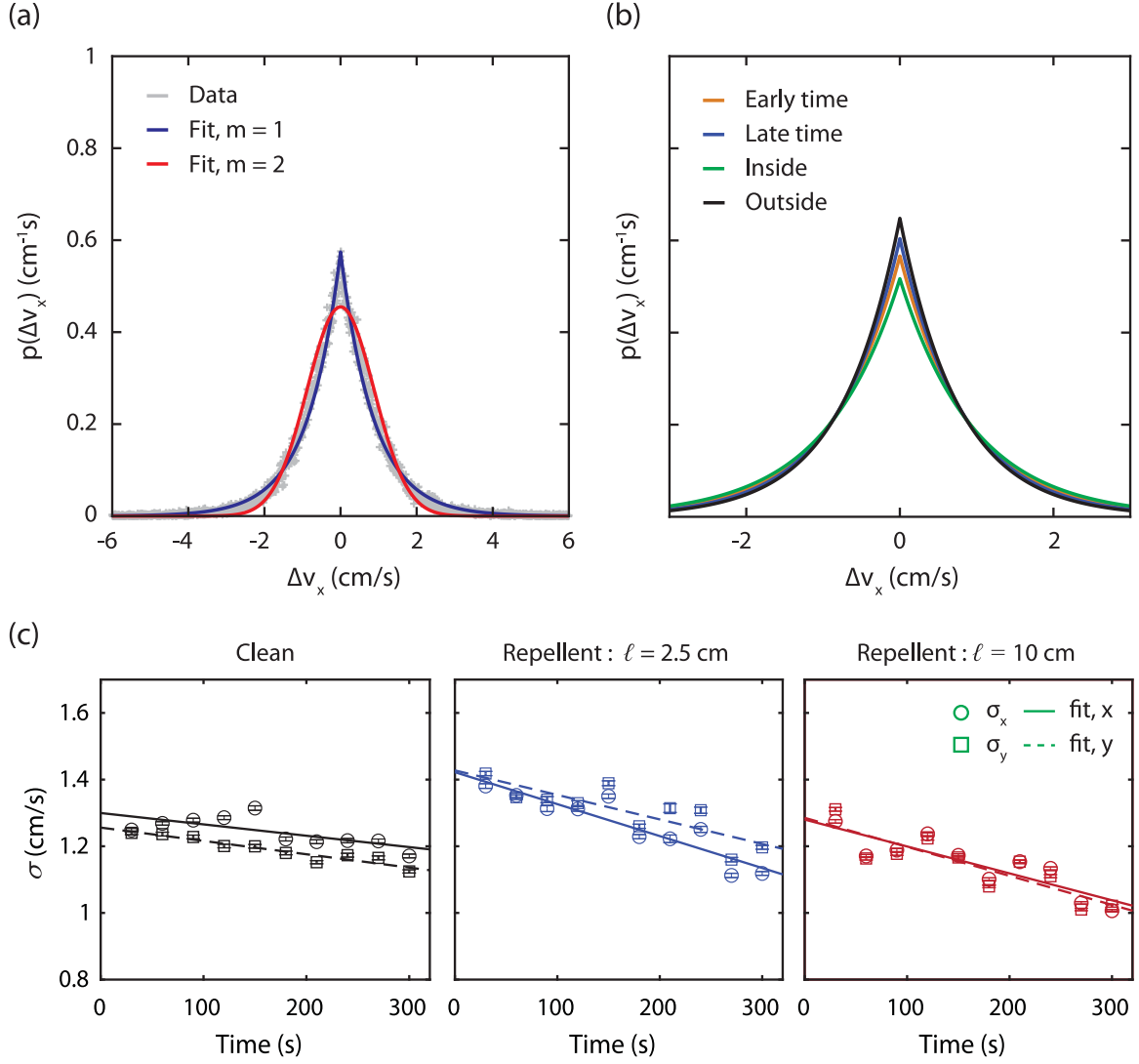


FIG. 4. (a) The data for the probability distribution $p(\Delta v_x)$ in a clean arena and a fit to Eq. (2) with $m = 1$ (blue) and the $m = 2$ (red). (b) More $m = 1$ fits to $p(\Delta v_x)$ for various data subsets, including early times (orange), late times (blue), inside (green) and outside (black) the region with chemical repellent. (For noncolor plots, curves from top to bottom are black, blue, orange, green.) For the latter, repellent was in zone \mathcal{R} with width $\ell = 10$ cm. (c) σ_x (circle) and σ_y (square) change over time for all ants in a clean arena (black) and with repellent in zone \mathcal{R} of width $\ell = 2.5$ cm (blue) and $\ell = 10$ cm (orange).

clean arena with position $|x|, |y| < L/2 - d$, along with the complementary subsets for positions $|x|, |y| > L/2 - d$ from the boundary strip. Finally, with the repellent coated over zone \mathcal{R} , length $\ell = 10$ cm and $\ell = 2.5$ cm, we show results for positions in and out of this repellent.

The first observation is that the distributions are qualitatively robust. The goodness of fit, indicated by χ^2 does not change drastically. As evident from Figs. 3 and 4, the expression Eq. (2) has the same qualitative behavior as the data when $m = 1$. We note that a Gaussian with $m = 2$ gives a significantly worse quantitative fit and has the wrong qualitative shape. The Pearson correlation coefficient ρ , which measures the correlation between velocity changes at nearby time steps, is always small. The size of σ^2 is roughly constant.

We chose the value of σ to minimize χ^2 , which evaluates goodness of fit. We do not expect a quantitative fit and are less concerned with the absolute value of χ^2 than with its change from subset to subset. But for completeness we note that if

Eq. (2) is the probability distribution for a velocity change $\Delta v_x = \eta$ then out of M data points, $\bar{M}(\eta) = M p(\eta) \Delta \eta$ are expected to land in a bin of width $\Delta \eta$ centered on η . If the measured number in this histogram bin is $M(\eta)$ then

$$\chi^2 = \sum_{\eta} (M(\eta) - \bar{M}(\eta))^2 / \bar{M}(\eta), \quad (7)$$

where the sum is over the $N_{\text{bins}} = 500$ values of η used. This quantity measures the deviation between the measured and expected histograms under the assumption that Eq. (2) is the true probability distribution of velocity change.

A basic assumption of our model is that each impulse $\eta(t)$ is an independent random variable. The correlation coefficients in Table I are $\rho = \rho(\Delta v_x[t], \Delta v_x[t + 3\Delta t])$ and $\rho = \rho(\Delta v_y[t], \Delta v_y[t + 3\Delta t])$ in respective columns, where

$$\rho(X, Y) = \frac{\{(X - \{X\})(Y - \{Y\})\}}{(\{X^2\} - \{X\}^2)^{1/2}[(\{Y^2\} - \{Y\}^2)^{1/2}]} \quad (8)$$

TABLE I. The results of fitting the measured distribution of velocity changes $p(\Delta v_x)$ and $p(\Delta v_y)$ for various data subsets to Eq. (3) with $m = 1$. The labels “early” and “late” refer to times $t < 30$ s and $t > 270$ s, while “interior” means $|x|, |y| < L/2 - d$ and $x \approx L/2$ means $L/2 - d < |x| < L/2$. When repellent is present in zone \mathcal{R} , with width ℓ in cm, the “in” label means $|x| < \ell/2$, “out” means $|x| > \ell/2$, and $x \approx 0$ means $|x| < 1.25$ cm. The fitting parameter σ^2 had a typical uncertainty $\Delta\sigma^2 \approx 0.02 \text{ cm}^2 \text{ s}^{-2}$ with a maximum $0.05 \text{ cm}^2 \text{ s}^{-2}$ in the repellent for $\ell = 2.5$ cm. The goodness of fit, reflected by the dimensionless χ^2 value, is discussed in the text, as is the dimensionless Pearson correlation coefficient ρ .

Subset	$p(\Delta v_x)$			$p(\Delta v_y)$		
	$\sigma^2 \text{ cm}^2 \text{ s}^{-2}$	χ^2	$10^2 \rho$	$\sigma^2 \text{ cm}^2 \text{ s}^{-2}$	χ^2	$10^2 \rho$
Overall	1.51	2	-2	1.41	2	-1
Early	1.55	8	0	1.53	10	0
Late	1.37	16	1	1.26	12	2
Interior	1.29	3	-4	1.35	3	-4
$ x \approx L/2$	1.38	3	0	2.07	2	2
$ y \approx L/2$	1.83	1	1	1.11	2	-1
$\ell = 10$, in	1.87	4	1	1.48	18	-2
$\ell = 10$, $x \approx 0$	1.93	2	-1	1.46	2	1
$\ell = 10$, out	1.17	2	-1	1.23	2	-1
$\ell = 2.5$, in	2.64	1	4	1.80	3	2
$\ell = 2.5$, out	1.52	22	-2	1.69	19	-1

and the curly brackets denote an average over the subset. We considered times separated by $3\Delta t$ because those closer together are constructed using overlapping data points $\mathbf{r}(t)$. Since $\{\Delta v_x(t)\} = \{\Delta v_x(t + 3\Delta t)\} \approx 0$ and $\{(\Delta v_x[t])^2\} = \{(\Delta v_x[t + 3\Delta t])^2\} \approx \sigma^2$, the value of $\rho = \{\Delta v_x(t)\Delta v_x(t + 3\Delta t)\}/\sigma^2$ indicates the size of the correlation of impulses at nearby time steps compared to their magnitude at each step. The fact that $\rho \ll 1$ suggests that it is reasonable to treat the impulses as independent.

Quantitatively, differences are seen in the parameters of Table I. For example, the square symmetry is not perfect, since σ_y is smaller than σ_x in the clean arena. The effect is larger than would occur by chance (the difference between σ_x^2 and σ_y^2 is ten times greater than uncertainty, which is $0.01 \text{ cm}^2 \text{ s}^{-2}$ for both) but small enough that it does not threaten the assumption that the navigation algorithm is local. Since ants regard the x and y directions as roughly equivalent, they are not using the sight (or smell) of a distant landmark as their primary guide.

B. Time and position dependence of random motion

According to Table I and Fig. 4(c), σ decreases with time t . This is detailed in Table II, which gives results of linear fits to σ versus t . For a clean arena, the downward trend is weak: the slope of σ_y versus t is zero within uncertainty. In an arena with repellent, σ decreases more significantly since the slope is several times larger than its uncertainty. This could be an indication that ants learn to move a bit more cautiously over time in the presence of repellent. But the main point here is that σ does not change substantially over the duration of the experiment.

Also from Table I, there is a sizable difference in the value σ^2 obtained for positions near the boundary compared to those

TABLE II. A linear regression was done on the data Fig. 4(c), in which σ values are plotted vs time t . The slope $m = \Delta\sigma/\Delta t$ and its uncertainty are indicated for σ obtained from Δv_x and Δv_y in the clean arena and that with repellent present.

	$10^3 m_{\sigma,x} \text{ cm}^2 \text{ s}^{-2}$	$10^3 m_{\sigma,y} \text{ cm}^2 \text{ s}^{-2}$
Clean	-0.3 ± 0.1	-0.4 ± 0.4
$\ell = 2.5$ cm	-0.9 ± 0.1	-0.7 ± 0.2
$\ell = 10$ cm	-0.8 ± 0.2	-0.9 ± 0.2

for the interior. While the difference is an order of magnitude larger than the uncertainty in σ^2 , it is certainly influenced by the ant-boundary interaction. The field term in Eq. (1) is strong in the boundary strips, so we cannot ignore it and expect to get a reliable value of σ when fitting Δv_x , Δv_y distributions to Eq. (2). Ant behavior near the boundary is not a good indication of natural behavior so it is not our main interest [37].

Finally, the value of σ is larger in zone \mathcal{R} when repellent is present. Again the difference is far greater than the statistical uncertainty in σ^2 . If the fit value of σ could be wholly attributed to random impulses, then an enhancement of σ would be interesting in light of what is known about chemotaxis by bacteria and other organisms. Bacteria that move according to the “run and tumble” technique vary the frequency at which they tumble depending on the local environment [24,38–41]. Ants could plausibly adjust their σ value, modifying their random walk characteristics, when they find themselves in an unpleasant region.

However, the apparent increase in the best-fit value of σ in zone \mathcal{R} is sensitive to field effects. According to the model, the ant suffers a velocity change as it overcomes a potential barrier. Because of this, $\{\Delta v_x^2\}$ should be large for a subset of data localized at the border of zone \mathcal{R} . Naively fitting $p(\Delta v_x)$ to Eq. (2) would result in an inflated σ value. So ant chemotaxis, via the modification of σ in response to the repellent, is not easy to see in our data. We now turn to deterministic effects, which are clearer.

C. Deterministic motion

1. Time-dependent squared velocity

The model predictions for the average squared velocity $\{v_{\parallel}^2\}$ and $\{v_{\perp}^2\}$ among an ensemble of ants, which entered the interior of a clean arena at time $t = 0$, is shown in Fig. 5. Here v_{\parallel} is the velocity component parallel to the boundary strip from which the ant entered and v_{\perp} is perpendicular to it. The initial value of $\{v_{\perp}^2\}$ is small, since members recently stopped at the boundary, but $\{v_{\parallel}^2\}$ is large because ants move rapidly along the boundary. While $\{v_{\perp}^2\}$ initially increases because random impulses accelerate ants, it later decreases because the fastest ants leave the arena interior first, reducing the average velocity among those that remain. In contrast $\{v_{\parallel}^2\}$, large initially, decreases monotonically because of the latter effect.

The velocities are expressed in units of v_{∞} in Fig. 5(b). We have a rough estimate $v_{\infty} = 5.3 \text{ cm/s}$ from the shoulder feature in Fig. 3. Using this and $\sigma_x^2 = 1.51 \text{ cm}^2 \text{ s}^{-2}$, we get

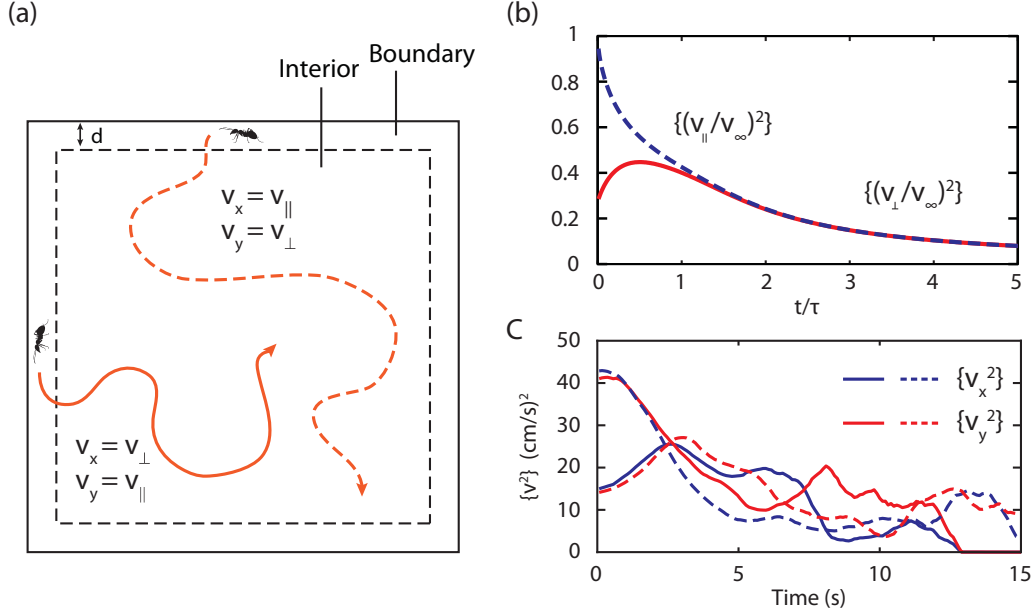


FIG. 5. (a) Cartoon illustrating the meaning of the velocities v_{\parallel}^2 and v_{\perp}^2 for solid and dashed curves. We calculated and measured ensemble averages of these quantities as functions of time in the clean arena. (b) Model prediction: $\{v_{\parallel}^2\}$ (blue dashed curve) and $\{v_{\perp}^2\}$ (red solid curve) calculated for model ants. Time is in units of τ and velocity in units v_{∞} . (c) Experimental result for ants in the clean arena. As in (a) ants entered the interior from $|x| = L/2 - d$ for solid curves and $|y| = L/2 - d$ for dashed curves.

a basic time scale $\tau = 2.4$ s and length scale $v_{\infty}\tau = 12.8$ cm for the model. The size of the arena L is comparable to $v_{\infty}\tau$, so ants come close to achieving equilibrium in the arena interior.

The corresponding experimental quantity is shown in Fig. 5(c), with $\{v_x^2(t)\}$ and $\{v_y^2(t)\}$ plotted for ants entering the interior from all edges. The velocity components perpendicular to the boundary follow the same trend as the model prediction for v_{\perp} while parallel components behave similarly to v_{\parallel} . Of course, the model does not capture the noisy behavior of the experimental curves, especially at large times where the ensembles are depleted and data describe the erratic behavior of a small number of ants.

Seeing that qualitative features of the model and data are similar, we attempt a quantitative comparison. From the initial value of $\{v_{\parallel}^2\}$, we get $v_{\infty} \approx 6.5$ cm/s, which is a bit larger than the value suggested by the shoulder feature. The time of the peak in $\{v_{\perp}^2(t)\}$ occurs at time $t/\tau \approx 0.5$ in the model and closer to $t \approx \tau$ in the experiment. So, we have agreement to within a factor of order unity in both cases.

2. Position dependence of squared velocity

The model position dependence of $\{v_x^2\}$ and $\{v_y^2\}$ is sketched in Fig. 6. These quantities approach v_{∞}^2 in the open arena but are depressed at the boundary and border to zone \mathcal{R} . Notably, they approach the same equilibrium value within zone \mathcal{R} , in the repellent, as in clean regions. Once a model ant overcomes the potential and arrives in zone \mathcal{R} , it forgets about this experience and random impulses restore its speed to v_{∞} .

Experimentally, $\{v_x^2\}$ and $\{v_y^2\}$, shown in Fig. 6, are qualitatively consistent with the model predictions. For the clean arena, $\{v_x^2\}$ is small near the edges then rises to a maximum and becomes weakly position-dependent near the middle of

the arena. The maximum $\sqrt{\{v_x^2\}} \approx 5.4$ cm/s gives another experimental estimate of v_{∞} that is consistent with previous values. The x dependence of $\{v_y^2\}$ is dominated by boundary effects: near $x = \pm L/2$ most ants are moving quickly along the edges and $\sqrt{\{v_y^2\}} \approx 4.8$ cm/s is close to v_{∞} . Near $x = 0$, a large fraction of ants move rapidly along $y = \pm L/2$ with a small v_y component, so $\{v_y^2\}$ is reduced.

The repellent causes disturbances in $\{v_x^2\}$ at the borders to zone \mathcal{R} but has no noticeable effect on $\{v_y^2\}$. When $\ell = 2.5$ cm, we see a depression in $\{v_x^2\}$ in zone \mathcal{R} . The expected recovery within zone \mathcal{R} is, perhaps, seen from the small peak occurring right at $x = 0$. This recovery is more clearly seen when $\ell = 10$ cm, as $\{v_x^2\}$ has minima at the borders to zone \mathcal{R} and increases to either side of it.

We can see, from Fig. 6, why shoulder features were missing from the distribution of v_x when repellent was present in zone \mathcal{R} , width $\ell = 10$ cm. Ants do not have enough space free from disturbances, between the arena boundary and the borders to zone \mathcal{R} , to achieve equilibrium velocity.

3. Field and potential

Supposing that the ant cannot leave the arena, the boundary is associated with an infinitely high potential barriers. For the repellent, we use a square potential barrier of height V_0 . The associated field $E_x = -dV/dx$ is a pair of δ -function spikes, of opposite sign, at the borders to zone \mathcal{R} . These are depicted in Fig. 7. We gave the spikes finite width.

The experimental field $E_x(x)$ is obtained by ordering experimental data according to x and taking a running average over Δv_x . The potential is obtained by integrating the field. The results are shown in Fig. 7(a). For the clean arena (not shown) the x -averaged value of Δv_x , interpreted as the field

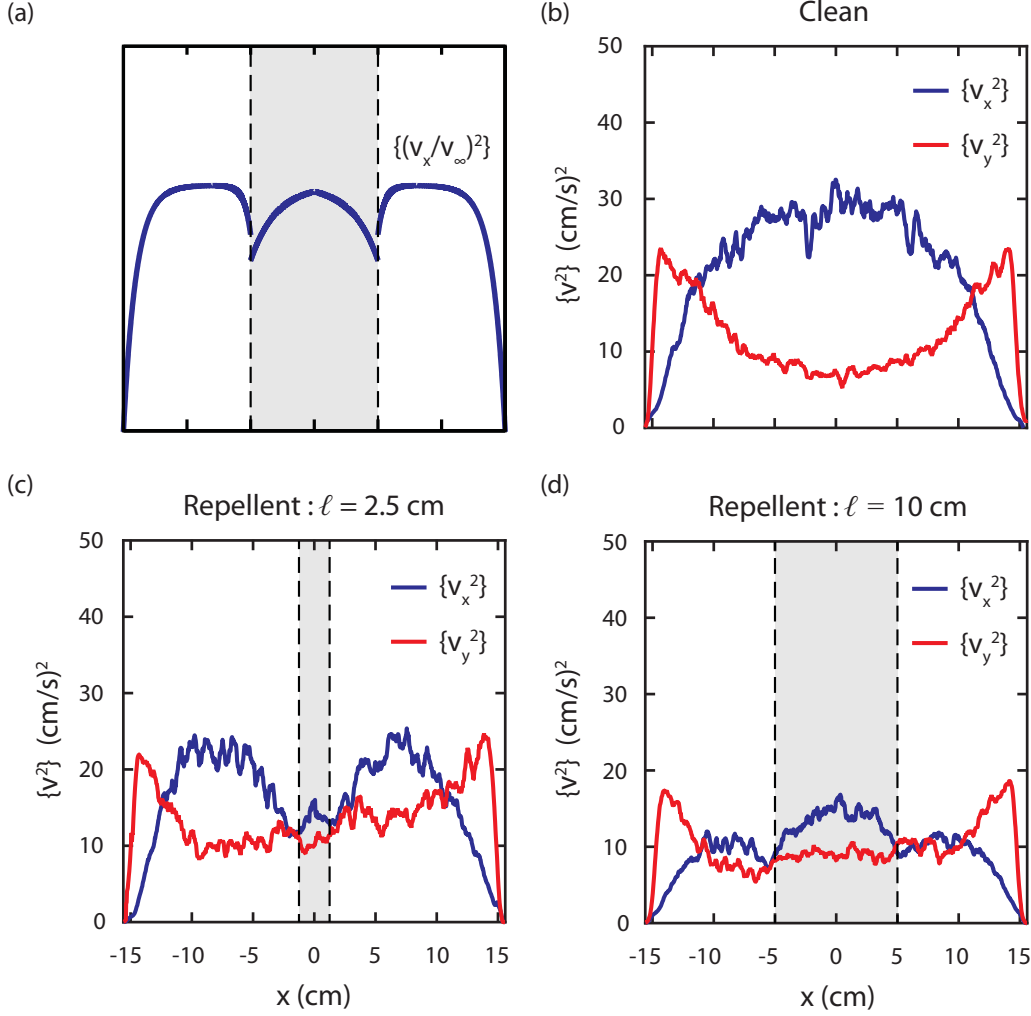


FIG. 6. (a) Rough sketch of the x -dependent value of $\{v_x^2\}$ predicted for the model with repellent in zone \mathcal{R} . The plateau height is $v_x = v_\infty^2$. Experimental results for $\{v_x^2\}$ and $\{v_y^2\}$ for (b) a clean arena, (c) with repellent in zone \mathcal{R} with width $\ell = 2.5$ cm and (d) with $\ell = 10$ cm.

E_x , is close to zero in the interior. At the boundaries E_x is large over a short range, directed into the arena. These boundary fields, seen at $x = \pm L/2$ in Figs. 7(b) and 7(c), look the same without or with repellent.

With repellent in zone \mathcal{R} , we see spikes in the measured E_x at the borders to zone \mathcal{R} . Their finite width can be attributed to several factors. For one, the border to zone \mathcal{R} is not perfectly straight in reality. For a more interesting one, the ant has finite spatial resolution in its determination of the field that varies according to the speed and angle at which it crosses into zone \mathcal{R} . The experimental potential $V(x)$ is also plotted. A square barrier, roughly resembling the ideal model, is seen when the width of zone \mathcal{R} is $\ell = 10$ cm. In the case of $\ell = 2.5$ cm, the square barrier has narrowed to a peak.

The experimental values for the height of the potential barrier V_0 fall in the range of $0.3\text{--}0.7\text{ cm}^2\text{ s}^{-2}$. This is likely an underestimate of the barrier height. Determining the field and potential in this manner is numerically delicate: one has to choose bins for the running average that are big enough to ensure random impulses average to zero but small enough to preserve some spatial resolution.

4. Crossing probability and residence time

The crossing probability P_C and time T_R spent continuously in zone \mathcal{R} were discussed above. According to the model calculations, described in Appendix B, P_C decreases with barrier size V_0 because ants are slowed as they enter zone \mathcal{R} . For the clean arena, $V_0 = 0$, so P_C is reduced by the presence of the repellent. The same slowing effect results in an initial increase in T_R with V_0 , so a weak repellent will increase the time ants spend in zone \mathcal{R} as compared to a clean region of the same size. With a sufficiently large V_0 , T_R decreases because ants are immediately repelled.

We measured P_C and T_R for the data subset in which the ant entered zone \mathcal{R} with position $|y| \leq L/2 - d$, to reduce boundary effects, and give the values in Table III. The crossing probability is lower when repellent is present. But ants reside within zone \mathcal{R} for a longer time when it is contaminated with the chemical repellent than when clean. This counterintuitive behavior agrees with the model prediction.

It should be emphasized that the quantitative values of P_C and T_R calculated using our model (see Appendix B for details) do not agree with the data. For $\ell = 10$ cm and

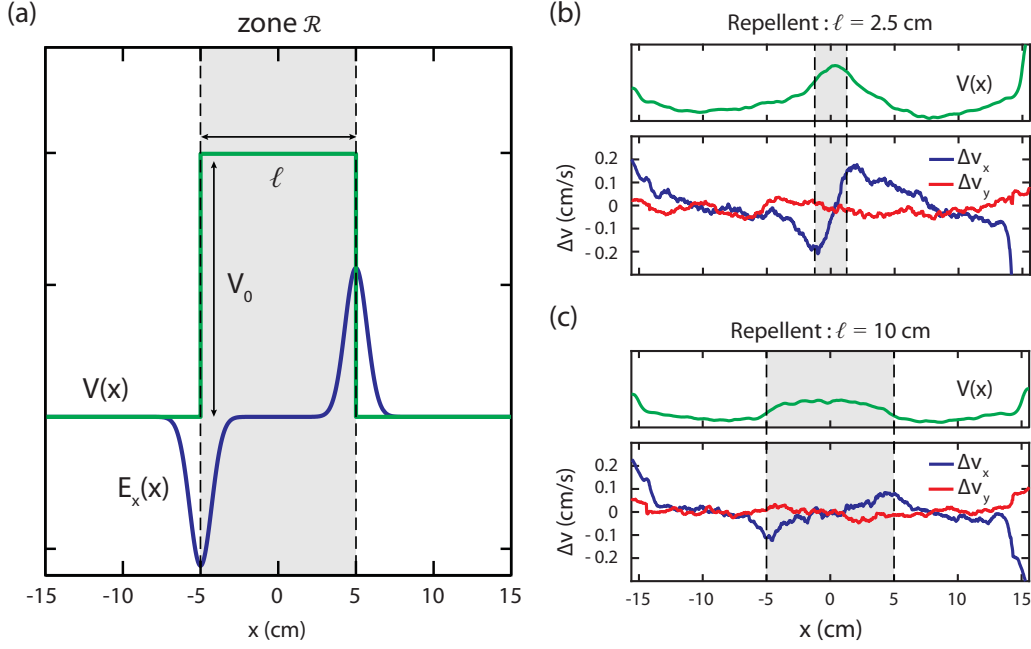


FIG. 7. (a) Model assumption for the field and potential $V(x)$ vs position x , showing V_0 in zone \mathcal{R} . The vertical scale is arbitrary. Experimental results, running averages of Δv_x (blue) and Δv_y (red) along with the potential (green) vs position x with repellent when (b) $\ell = 2.5$ cm and (c) $\ell = 10$ cm.

$\ell = 2.5$ cm, the model predictions of $P_C = 0.7$ and $P_C = 0.92$ are smaller than measured values. The residence times T_R , calculated using the crude but simplifying continuum approximation to the discrete random walk, were an order of magnitude smaller than measured values. But the qualitative effect of repellent on P_C and T_R is notable.

D. Summary

The simplistic theoretical model accounts for almost all statistical properties of ant motion in the experiment. Recall that the model includes a constant probability distribution $p(\eta)$ for random impulses, with zero mean, mean-square σ^2 , and negligible time correlations. It also includes a field due to interactions with the boundary and the chemical repellent, where the latter can be adequately modeled by a scalar potential that has a positive value V_0 if repellent is present and is zero elsewhere. The navigation algorithm implied by this model is purely local, i.e., ants modify their path in response to

their current position and velocity, without taking into account distant surroundings.

The theory is characterized by a small number of parameters: say v_∞ , σ^2 and V_0 , the first two of which are obtained from data for the clean arena. It provides a scheme for simulating motion in more general conditions.

V. CONCLUSIONS

The motion of individuals belonging to the species *Oecophylla smaragdina* of weaver ants was studied in a small square arena by measuring the ant position as a function of time. The arena was a tile that was either clean, or with a defined region coated with citronella oil, a substance that repels ants. The aim was to determine a simple underlying algorithm that governs ant navigation, in particular the method they use to avoid the repellent.

We found that a version of the Langevin theory of Brownian motion provides a good description of statistical properties of the data. The equation of motion for ants is Newton's second law with a random force, with zero time average and a fixed, robust probability distribution function $p(\eta) e^{-|\eta|}$ giving uncorrelated random impulses that act at each time step. The repellent can be modelled by an effective potential energy, and associated field, that results in ants receiving a negative impulse when they enter the region coated with repellent.

Most aspects of the data can be adequately accounted for with this minimal model, including counterintuitive properties like the fact that ants spend more time continuously within a region with repellent present than they would in a clean region of the same size. The algorithm may be used to simulate motion, allowing investigations of more complex properties of motion to be done computationally.

TABLE III. The measured probability P_C that an ant crosses zone \mathcal{R} , length ℓ , and measured time T_R it remains continuously in zone \mathcal{R} . Both depend on whether zone \mathcal{R} has no repellent, i.e., is “clean” or is coated evenly with the repellent citronella oil, “repel.” Statistical error in P_C and T_R were about 0.02 and 0.05 s, respectively.

	P_C	T_R (s)
$\ell = 10$ cm $\begin{cases} \text{clean} \\ \text{repel} \end{cases}$	0.91 ± 0.03	1.85 ± 0.08
	0.51 ± 0.04	2.08 ± 0.08
$\ell = 2.5$ cm $\begin{cases} \text{clean} \\ \text{repel} \end{cases}$	0.95 ± 0.02	0.52 ± 0.02
	0.79 ± 0.03	0.87 ± 0.04

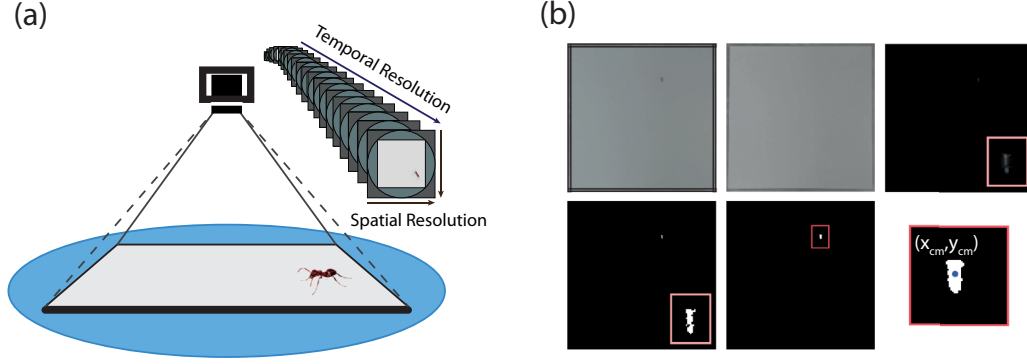


FIG. 8. The image processing steps used for tracking weaver ant motion. (a) Imaging: data saved as a digital image sequence with a certain spatial resolution (limited by square pixel length Δx) and temporal resolution (limited by frames per second $1/\Delta t$) over a total duration of 300 s. (b) In-house algorithms isolate and identify the ant position and assign it spatial coordinates (the position of the optical center of mass) by removing it from of an individual ant from the background, as further detailed in the text.

ACKNOWLEDGMENTS

Funding was provided by Suranaree University of Technology (SUT). T.T. was supported by a Graduate Research Fund (Kittibandit) and P.P. by the Development and Promotion of Science and Technology Talents (DPST), Thailand.

APPENDIX A: IMAGE PROCESSING

1. Insects

We used multiple colonies of weaver ants, *Oecophylla smaragdina*, which were captured at Suranaree University of Technology, Nakhon Ratchasima, Thailand ($14^\circ 52' 22.5''\text{N}$, $102^\circ 1' 25.32''\text{E}$). We used a clean plastic box to capture a single ant and transported it to the laboratory without touching it.

2. Experimental setup

Before video recording, we placed the ant gently in the arena. The arena is a $30 \times 30 \times 0.6 \text{ cm}^3$ ceramic floor tile, with the large face horizontal. It is partly submerged in water. The water surface is 0.1 cm below the top of the tile, so ants that reach the edge of the tile encounter this short drop into water. They rarely attempt to leave the tile. We maintained a temperature of 25°C during the video recording in the laboratory. Each ant underwent a single trial, lasting 5 min. Its motion was recorded using a digital HD video camera (digital sampling rate of 30 frames per second).

3. Image processing

In this process, we tracked the ant position using a MATLAB program and image-tracking process as follows:

- (1) Import a color image of each frame of the video and select an image that includes the centered square plate and a rim, of width 0.5 cm, of surrounding water.
- (2) Convert each color image to a gray scale and construct a background image by averaging over all frames.
- (3) From each gray scale image, we subtract the background. This gives us a picture of the ant.
- (4) Adjust the intensity (contrast and saturation) of the resulting image to see the ant more clearly and then convert each gray scale image to a binary image (black-white scale) by choosing a suitable intensity threshold.

- (5) To reduce noise, remove all points that are significantly bigger or smaller than the average ant size.

- (6) We identify a spatial coordinate $\mathbf{r}(t) = (x(t), y(t))$ at each time step using the mean of the binary function.

Note that, we extract a spatial position of an ant using two consecutive frames. This means that $\Delta t = 2/30 \text{ s}$ is the smallest time step we can use. According to the spatial resolution of the camera, $x = 0.03 \text{ cm}$ per pixel is the smallest distance we can resolve. In Fig. 8, these image processing steps are illustrated.

To fit the measured probability distribution of velocity changes $p(\Delta v_x)$ and $p(\Delta v_y)$, we initially used both parameters σ and m appearing in Eq. (3). For given values of σ and m the value of $\chi^2 = \chi^2(\sigma, m)$, which we defined in Eq. (7), was calculated. In Fig. 9 we show χ^2 over a range $0 < \sigma < 3$ and $0 < m < 2$ for the case where $|x|, |y| < L/2 - d$ in a clean arena (this is a subset free from boundary effects). The red dot in the figure indicates the point σ, m where χ^2 is minimum.

There is a valley in Fig. 9, surrounding the minimum, in which χ^2 remains fairly close to its minimum value. We take advantage of this by fixing $m = 1$ and finding the σ that minimized χ^2 . That is, we approximated the best two-parameter fit by the best one-parameter fit with $m = 1$. A Gaussian, $\sigma = 2$ lies outside this valley and, moreover, Gaussian fits do not have the appropriate qualitative shape near the origin.

APPENDIX B: THEORETICAL MODEL

Here we more fully develop the model sketched in Sec. III and use it to calculate several measurable properties of ant motion. These are all ensemble averages, which can be approximated without using simulations of the random motion. Because of the square symmetry of the arena, the motion along x and y are independent. Many quantities can be obtained in a one-dimensional picture and the generalization to two dimensions is straightforward.

Consider a large ensemble of ants moving in one dimension with their velocities determined by one component of Eq. (1). The ensemble has a probability distribution $\Pi(x, v, t)$ over position x , velocity v , at time t . A normalized probability distribution over position (velocity) alone is obtained by integrating $\Pi(x, v, t)$ over all velocity (position). The average

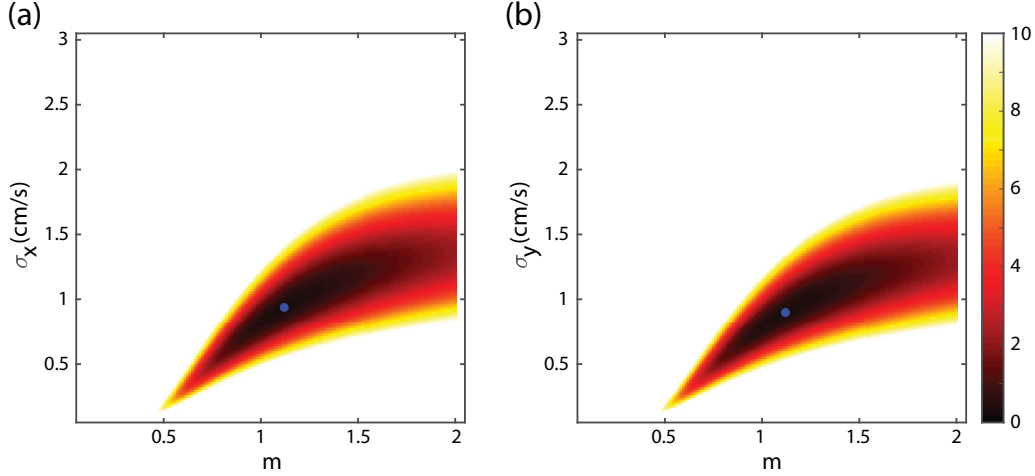


FIG. 9. The χ^2 value, obtained from fits of the experimental histograms of (a) $p(\Delta v_x)$ and (b) $p(\Delta v_y)$ to Eq. (2), is color-plotted as a function of the two free parameters m and σ of Eq. (2). Darker color indicates a smaller value of χ^2 and thus a better fit. The optimal values (a) $m = 1.12$ and $\sigma_x = 0.94$ cm/s, (b) $m = 1.12$ and $\sigma_y = 0.90$ cm/s, are indicated by blue dots. Since χ^2 remains comparably small over a broad region in (m, σ) , it is convenient to fix $m = 1$ and use σ as the only parameter.

of a function $f(x, v, t)$ at time t is

$$\{f(t)\} = \int_{-\infty}^{\infty} dx \int_{-\infty}^{\infty} dv \Pi(x, v, t) f(x, v, t). \quad (\text{B1})$$

Of particular interest are mean values $\{v(t)\}$, $\{x(t)\}$, and variances

$$\begin{aligned} \sigma_v^2(t) &= \{v^2(t)\} - \{v(t)\}^2, \\ \sigma_x^2(t) &= \{x^2(t)\} - \{x(t)\}^2. \end{aligned} \quad (\text{B2})$$

Suppose that each member of the ensemble begins with $x(0) = x_0$, and $v(0) = v_0$ in an infinite, clean arena. The velocity and position change as $v(t + \Delta t) = v(t) - v(t)\Delta t/\tau + \eta(t)$ and $x(t + \Delta t) = x(t) + v(t)\Delta t$, where $\eta(t)$ is a random variable, with a probability distribution $p(\eta) = p(-\eta)$. Thus $\{\eta\} = 0$ and $\{\eta^2\} \equiv \sigma^2$ where σ is the standard deviation of random impulses. In an ensemble average, terms odd in η vanish so $\{v(t + \Delta t)\} - \{v(t)\} = -\{v(t)\}(\Delta t/\tau)$. In the $\Delta t \rightarrow 0$ limit this becomes $d\{v\}/dt = -\{v\}/\tau$. In the same way, we find $d\{v^2\}/dt = -2\{v^2\}/\tau + \sigma^2/\Delta t$, $d\{xv\}/dt = -xv/\tau + \{v^2\}$, $d\{x\}/dt = v$, $d\{x^2\}/dt = 2\{xv\}$ that can all be integrated.

In writing the solution $\{v^2(t)\} = v_\infty^2 + (v_0^2 - v_\infty^2)e^{-2t/\tau}$, we introduce a terminal speed v_∞ defined by $v_\infty^2 = \sigma^2\tau/(2\Delta t)$. Velocity will now be written in units of v_∞ , time in units of τ and distance in units of τv_∞ so all three variables become dimensionless. The mean values are $\bar{v}(t, v_0) = \{v(t)\} = v_0 e^{-t}$ and

$$\bar{x}(t, x_0, v_0) = \{x(t)\} = x_0 + v_0(1 - e^{-t}) \quad (\text{B3})$$

and the standard deviations given by

$$\sigma_v^2(t) = 1 - e^{-2t}, \quad \sigma_x^2(t) = -3 + 2t + 4e^{-t} - e^{-2t}. \quad (\text{B4})$$

At large t the spread in velocity $\sigma_v(t) \rightarrow 1$ while σ_x increases without bound in an infinite arena. Note that after a time $t \approx \tau$ an ant forgets its initial state and approaches its equilibrium velocity. After moving a distance $d \approx v_\infty\tau$ away from a disturbance, it similarly approaches equilibrium.

We will write $G(x; \bar{x}, \sigma)$ for a normalized Gaussian in the variable x , with mean \bar{x} and standard deviation σ . The initial distribution can then be written $\Pi_0(x, v) = \Pi(x, v, 0) = \delta(x - x_0)\delta(v - v_0) = G(x; x_0, \epsilon)G(v; v_0, \epsilon)$ using a particular representation of a delta function with an infinitesimal quantity ϵ . The equilibrium distribution for the infinite arena is $\Pi(x, v, \infty) = \Pi_\infty(v) = G(v; 0, 1)$. To approximate time evolution of an ensemble, replace Gaussian parameters with time-dependent values that give the mean and standard deviation found above. Thus the time-dependent distribution is

$$\Pi(x, v, t) = G(x; \bar{x}[t, x_0, v_0], \sigma_x[t])G(v; \bar{v}[t, v_0], \sigma_v[t]) \quad (\text{B5})$$

when $\Pi_0(x, v) = \delta(v - v_0)\delta(x - x_0)$. An arbitrary initial distribution is first written as

$$\Pi_0(x, v) = \int_{-\infty}^{\infty} dx' \int_{-\infty}^{\infty} dv' \Pi_0(x', v') G(x; x', \epsilon) G(v; v', \epsilon) \quad (\text{B6})$$

and primed variables treated as initial values to get

$$\begin{aligned} \Pi(x, v, t) &= \int_{-\infty}^{\infty} dx' \int_{-\infty}^{\infty} dv' \Pi_0(x', v') \\ &\quad \times G(x; \bar{x}[t, x', v'], \sigma_x[t]) G(v; \bar{v}[t, v'], \sigma_v[t]). \end{aligned} \quad (\text{B7})$$

In two dimensions, the distribution function is $\Pi(x, v_x, t)\Pi(y, v_y, t)$ and Eq. (B7) generalized to include integrals over y', v'_y with two more Gaussians of the same form.

The results above apply to a clean, infinite arena. The effect of the field, which is important at the arena boundary and at the borders to zone \mathcal{R} when the chemical repellent is present, will be treated as initial values of these equations. The simplest model of the interaction with the boundary is to have ants stop abruptly at an edge and forget their previous

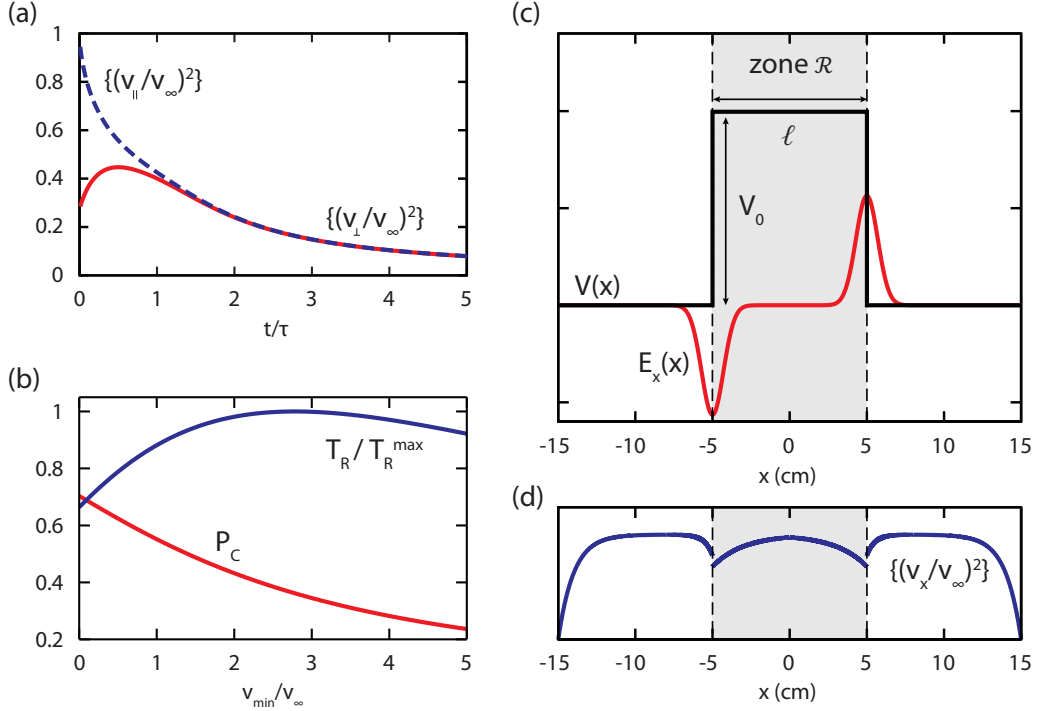


FIG. 10. Model predictions. (a) Plots of $\{v_{\perp}^2\}$ and $\{v_{\parallel}^2\}$ for ants in the interior vs time. (b) The crossing probability P_C and residence time T_R in zone \mathcal{R} plotted vs v_{\min}/v_{∞} where $v_{\min}^2 = 2V_0$. (c) The potential $V(x)$ vs position, showing V_0 in zone \mathcal{R} and the resulting field $E_x(x) = -dV/dx$. (d) A sketch of the average squared velocity vs position.

motion. When the ant reaches the boundary at $x = \pm L/2$ its velocity v_x drops to zero while its motion in the y direction is unaffected. For a clean arena that is sufficiently large, i.e., $L \gg 1$ (in units of τv_{∞}), ants far from boundary are in equilibrium.

First, consider the time dependence of the squared velocity of ants in the clean arena that have entered the central region, which is a square of length $L' = L - 2d$ centered in the arena of length L where $d \ll L$. An ant starting at the boundary $x = -L/2$ with $v_x = v_{\perp} = 0$ needs a typical time $t = t_1$ to reach the central region, which is found by inverting $\{x^2(t_1)\} = d^2$. The standard deviation of velocity at this time is $\sigma_1 = \sigma_v(t_1) \ll 1$. Only ants with $v_x > 0$ enter the central region from this side, so we use $G_+(x; \bar{x}, \sigma) = 2\theta(x)G(x; \bar{x}, \sigma)$ with $\theta(x < 0) = 0$ and $\theta(x > 0) = 1$, to write the distribution for members entering at $t = 0$ as $\Pi(x, v_x, 0) = \delta(x + L'/2)G_+(v_x; 0, \sigma_1)$. For motion along y we assume that most ants, being far from the boundary $y = \pm L/2$, are in equilibrium, so $\Pi(y, v_y, 0) = (1/L')\theta(L'/2 - |y|)G(v_y; 0, 1)$. The time evolution is introduced via Eq. (B7) and

$$\{v_{\alpha}^2(t)\} = \int_{-L'/2}^{L'/2} dx \int_{-L'/2}^{L'/2} dy \int_{-\infty}^{\infty} dv_x \int_{-\infty}^{\infty} dv_y \times v_{\alpha}^2 \Pi(x, v_x, t) \Pi(y, v_y, t), \quad (\text{B8})$$

where $\alpha = x, y$.

The results of Eq. (B8) appear in Fig. 10(a). At small times, $\{v_{\perp}^2(t)\}$ increases because ants accelerate as they move away from the boundary. After a time of order τ , it reaches a peak that is some fraction of v_{∞}^2 , then it starts to decrease.

Members that leave the central region are removed from the ensemble and, since fast ones leave first, $\{v_{\perp}^2(t)\}$ decreases. In contrast, the initial value $\{v_{\parallel}^2(0)\} = \{v_{\parallel}^2(0)\} = v_{\infty}^2$ is maximal, so $\{v_{\parallel}^2(t)\}$ decreases monotonically.

Next, we introduce the chemical repellent to the central zone \mathcal{R} , defined by $|x| < \ell/2$ where $\ell < L$, which adds a field $E_x(x)$ to Eq. (1). The effective potential $V(x) = V_0$ in zone \mathcal{R} and $V(x) = 0$ elsewhere. When an ant crosses into zone \mathcal{R} , it suffers an impulse $\Delta v_x = -v_{\min} = -2(V_0)^{1/2}$ opposite to the direction of its velocity. The potential results in a reduced density of ants in zone \mathcal{R} , since some are prevented from entering the zone.

Consider an ensemble approaching the border to zone \mathcal{R} . Since this border is far from the boundary, we assume the distribution is in equilibrium upon arrival at the border. While crossing into zone \mathcal{R} , some members are repelled by the barrier and the rest have their velocity reduced by v_{\min} . The resulting distribution, just after arriving into zone \mathcal{R} at $x = -\ell/2$ is $\Pi_0(x, v_x) = \delta(x + \ell/2)\theta(v_x)G(v_x + v_{\min}; 0, 1)$. This ensemble, which lost some members at the border, has to be normalized.

To calculate the crossing probability P_C and residence time T_R , we first find these quantities $P_C(x, v_x)$ and $T_R(x, v_x)$ for an ant with a certain initial position x and a certain velocity v_x . These functions can be weighted with the initial distribution to estimate their measurable values. The expected crossing probability is $P_C = \int dv_x \Pi_0(-\ell/2, v_x) P_C(-\ell/2, v_x)$ and residence time is $T_R = \int dv_x \Pi_0(v_x) T_R(-\ell/2, v_x)$, where we are using a 1D picture for simplicity.

The initial expected values of probability and residence time must be equal to their ensemble averages calculated one time step later, so

$$P_C(x, v_x) = \{P_C(x[\Delta t], v_x[\Delta t])\}, \quad (\text{B9})$$

$$T_R(x, v_x) = \Delta t + \{T_R(x[\Delta t], v_x[\Delta t])\}, \quad (\text{B10})$$

where the second equation has an extra term because the expected residence time remaining decreased the one time step. We substitute $x[\Delta t] = x + v_x \Delta t$ and $v_x[\Delta t] = v_x - v_x \Delta t / \tau + \eta$ then Taylor-expand in Δt and drop terms odd in η from the ensemble average. The first order terms vanish if the functions above depend on a single variable, i.e., if $P_C(x, v_x) = P_C(r)$ with $r = x + v_x \tau$ and the same for $T_R(x, v_x)$. The surviving terms up to second order result in

$$\partial^2 P_C / \partial r^2 = 0, \quad \partial^2 T_R / \partial r^2 = -1 \quad (\text{B11})$$

in dimensionless variables. With the boundary conditions $P(-\ell/2) = T(\ell/2) = T(\ell/2) = 0$ and $P(\ell/2) = 1$ we find

$$P_C(-\ell/2, v_x) = P_C(v_x) = v_x / \ell, \quad (\text{B12})$$

$$T_R(-\ell/2, v_x) = T_R(v_x) = v_x(\ell - v_x)/2. \quad (\text{B13})$$

These expressions are small-velocity approximations and meaningless for $v > \ell$. To crudely treat large velocities, we can set the crossing probability to 1 and residence time to 0 for $v_x > \ell$.

Since $P(v_x)$ is a monotonically increasing function of v_x , with the slowest ants having no chance of successfully crossing zone \mathcal{R} , the effect of the potential barrier is to reduce the typical initial velocity v_x and decrease P_C . The function $T_R(v_x)$ is nonmonotonic. It increases with velocity at small v_x , because slightly faster ants penetrate further into zone \mathcal{R} so it takes them longer to retreat back. It decreases at large v_x , because the fastest ants race through zone \mathcal{R} in less time. There is a corresponding nonmonotonic dependence of T_R on the potential barrier height. Consequently, a weak barrier potential V_0 will result in ants spending more time in zone \mathcal{R} than they would if $V_0 = 0$. That is, according to this model, ants will spend more time in a region with a mild repellent present than they would in a clean region of the same size.

Note that the quantitative value of P_C , obtained from this model, is considerably lower than the measured value. Also,

the predicted resident time T_R is much smaller than the measured value. The qualitative effect is illustrated in Fig. 10(b) by the plot of T_R normalized to its maximum value versus v_{\min} . For these plots we used $\ell = L/3$ and, wherever necessary, numerical values $v_\infty = 5.3$ cm/s and $\tau = 2.4$ s.

Finally, consider the dependence of $\{v_x^2(x)\}$ on position x in equilibrium (i.e., the time average of this quantity). It is obtained using Eq. (B1) with $\Pi(x, v_x, t)$ set equal to the equilibrium distribution. Again, we seek only a qualitative result. Since the equilibrium distribution does not change with time, it satisfies

$$v_x \partial \Pi / \partial x + (\partial v_x / \partial t) \partial \Pi / \partial v_x = 0. \quad (\text{B14})$$

To simplify the problem, we use a weak-field limit and assume the distribution is close to the zero-field equilibrium $\Pi_\infty(v_x)$, so $\Pi(x, v_x) = \Pi_\infty(v_x) + \Pi_1(x, v_x)$ where the second term, absent were it not for the field, is small. Equation (B14) becomes

$$\partial \Pi_1 / \partial x - E(x) \Pi_\infty(v_x) - \partial \Pi_1 / \partial v_x = 0, \quad (\text{B15})$$

where we dropped terms odd in η , used $v_x^2 = 1$ in the long time limit, and ignored terms like $E(x) \Pi_1(x, v_x)$ that are second order in the weak field. The field due to the repellent is $E(x) = -V_0 \delta(x + \ell/2) + V_0 \delta(x - \ell/2)$. It causes steplike jumps in the distribution $\Pi_1(\ell/2, v_x)$ at the borders to zone \mathcal{R} . Integrating Eq. (B15) over a small region centered on the border to \mathcal{R} gives

$$\int_{-\ell/2-\epsilon}^{-\ell/2+\epsilon} dx \partial \Pi_1 / \partial x = \Delta \Pi_1(-\ell/2, v_x) = -V_0 \Pi_\infty(v_x). \quad (\text{B16})$$

This is a localized disturbance caused by the field. As we move into the zero-field region, $\Pi_1(x, v_x)$ decays to zero and $\{v_x^2(x)\}$ approaches 1.

The zero-field version of Eq. (B15) is satisfied by any function $\Pi_1(x, v_x) = \Pi_1(x + v_x)$, so a possible form $\Pi_1(x, v_x) = \exp(-K[x + v_x - x_0]) \Pi_1(x_0)$ decays as we move away from a disturbance at x_0 . Ants moving out of zone \mathcal{R} receive an initial burst due to the force from the repellent and have a correspondingly larger slope K . The distribution at the boundary is $\Pi(-\ell/2, v_x) = \Pi(\ell/2, v_x) = \delta(v_x)$. We treat this as another localized disturbance that decays. This qualitative behavior is sketched in Fig. 10(d).

-
- [1] B. Holldobler and E. O. Wilson, *The Ants* (Harvard University Press, Cambridge, MA, 1990).
 - [2] B. Holldobler and E. O. Wilson, *Journey to the Ants: A Story of Scientific Exploration* (Belknap Press of Harvard University Press, Cambridge, MA, 1994).
 - [3] T. Sakiyama, Ant droplet dynamics evolve via individual decision-making, *Sci. Rep.* **7**, 14877 (2017).
 - [4] F. J. Vernerey, T. Shen, S. L. Sridhar, and R. J. Wagner, How do fire ants control the rheology of their aggregations? A statistical mechanics approach, *J. R. Soc., Interface* **15**, 20180642 (2018).
 - [5] A. C. Cole Jr., and J. W. Jones, A study of the weaver ant, *Oecophylla smaragdina*, *Am. Midl. Nat.* **39**, 641 (1948).
 - [6] B. Holldobler, Territorial behavior in the green tree ant (*Oecophylla smaragdina*), *Biotropica* **15**, 241 (1983).
 - [7] J. F. Kamhi, K. Nunn, S. K. Robson, and J. F. Traniello, Polymorphism and division of labour in a socially complex ant: neuromodulation of aggression in the Australian weaver ant, *Oecophylla smaragdina*, *Proc. R. Soc. London, Ser. B* **282**, 20150704 (2015).
 - [8] T. M. J. Golden and P. S. M. Hill, The evolution of stridulatory communication in ants, revisited, *Insectes Soc.* **63**, 309 (2016).
 - [9] A. Czirik, M. Vicsek, and T. Vicsek, Collective motion of organisms in three dimensions, *Phys. A (Amsterdam, Neth.)* **264**, 299 (1999).

- [10] T. Vicsek, A. Czirók, I. J. Farkas, and J. D. Helbing, Application of statistical mechanics to collective motion in biology, *Phys. A (Amsterdam, Neth.)* **274**, 182 (1999).
- [11] T. Vicsek and A. Zafeiris, Collective motion, *Phys. Rep.* **517**, 71 (2012).
- [12] P. DeLellis, G. Polverino, G. Ustuner, N. Abaid, S. Macrì, E. M. Bollt, and M. Porfiri, Collective behavior across animal species, *Sci. Rep.* **4**, 3723 (2014).
- [13] N. R. Franks, T. O. Richardson, S. Keir, S. J. Inge, F. Bartumeus, and A. B. Sendova-Franks, Ant search strategies after interrupted tandem runs, *J. Exp. Biol.* **213**, 1697 (2010).
- [14] B. Holldobler and E. O. Wilson, The multiple recruitment systems of the African weaver ant *Oecophylla longinoda* (Latreille) (Hymenoptera: Formicidae), *Behav. Ecol. Sociobiol.* **3**, 19 (1978).
- [15] D. M. Gordon, *Ant Encounters: Interaction Networks and Colony Behavior* (Princeton University Press, Princeton, 2010), Vol. 1.
- [16] T. Vicsek, A. Czirók, E. Ben-Jacob, I. Cohen, and O. Shochet, Novel Type of Phase Transition in a System of Self-Driven Particles, *Phys. Rev. Lett.* **75**, 1226 (1995).
- [17] F. Schweitzer, E. Ebeling, and B. Tilch, Complex Motion of Brownian Particles with Energy Depots, *Phys. Rev. Lett.* **80**, 5044 (1998).
- [18] G. M. Viswanathan, S. V. Buldyrev, S. Havlin, M. G. da Luz, E. P. Raposo, and H. E. Stanley, Optimizing the success of random searches, *Nature (London)* **401**, 911 (1999).
- [19] B. J. West and T. Nonnenmacher, An ant in a gurge, *Phys. Lett. A* **278**, 255 (2001).
- [20] D. W. Sims *et al.*, Scaling laws of marine predator search behaviour, *Nature (London)* **451**, 1098 (2008).
- [21] A. M. Reynolds, Distinguishing between Lévy walks and strong alternative models, *Ecology* **93**, 1228 (2012).
- [22] N. E. Humphries *et al.*, Environmental context explains Lévy and Brownian movement patterns of marine predators, *Nature (London)* **465**, 1066 (2010).
- [23] S. Bazazi, F. Bartumeus, J. J. Hale, and I. D. Couzin, Intermittent motion in desert locusts: behavioural complexity in simple environments, *PLoS Comput. Biol.* **8**, e1002498 (2012).
- [24] W. Bialek, *Biophysics: Searching for Principles* (Princeton University Press, Princeton, 2012).
- [25] P. Romanczuk, M. Bär, W. Ebeling, B. Lindner, and L. Schimansky-Geier, Active brownian particles, *Eur. Phys. J.: Spec. Top.* **202**, 1 (2012).
- [26] D. W. Sims, N. E. Humphries, R. W. Bradford, and B. D. Bruce, Lévy flight and Brownian search patterns of a free-ranging predator reflect different prey field characteristics, *J. Anim. Ecol.* **81**, 432 (2012).
- [27] D. A. Raichlen, B. M. Wood, A. D. Gordon, A. Z. P. Mabulla, F. W. Marlowe, and H. Pontzerf, Evidence of Lévy walk foraging patterns in human hunter-gatherers, *Proc. Natl. Acad. Sci. USA* **111**, 728 (2014).
- [28] P. Schultheiss, K. Cheng, and A. M. Reynolds, Searching behavior in social Hymenoptera, *Learn. Motiv.* **50**, 59 (2015).
- [29] M. J. B. Krieger, J.-B. Billeter, and L. Keller, Ant-like task allocation and recruitment in cooperative robots, *Nature (London)* **406**, 992 (2000).
- [30] C. R. Kube and E. Bonabeau, Cooperative transport by ants and robots, *Rob. Auton. Syst.* **30**, 85 (2000).
- [31] T. S. Deisboeck and I. D. Couzin, Collective behavior in cancer cell populations, *Bioessays* **31**, 190 (2009).
- [32] F. Esponda and D. M. Gordon, Distributed nestmate recognition in ants, *Proc. R. Soc. London, Ser. B* **282**, 20142838 (2015).
- [33] Y.-K. Chung and C.-C. Lin, Heat-induced symmetry breaking in ant (Hymenoptera: Formicidae) escape behavior, *PloS One* **12**, e0173642 (2017).
- [34] R. K. Pathria, *Statistical Mechanics* (Elsevier, Burlington, MA, 1996).
- [35] S. Wang, W. Lu, and S. Weigu, Behavior of ants escaping from a single-exit room, *PloS One* **10**, e0131784 (2015).
- [36] S. Wang, S. Cao, Q. Wang, L. Lian, and W. Song, Effect of exit locations on ants escaping a two-exit room stressed with repellent, *Phys. A (Amsterdam, Neth.)* **457**, 239 (2016).
- [37] One reason why ants tend to remain near the boundary could be that a one-dimensional structure like this allows an ant to explore a large region without becoming disoriented: humans would likely use the same strategy, following a river to avoid walking in circles. It is a large effect, from $\{v_x^2\}$ and $\{v_y^2\}$ plots in Fig. 5 it appears that ants move at high speed along the boundary and are subject to large impulses parallel to it as they do so.
- [38] R. M. Macnab and D. E. Koshland, The gradient-sensing mechanism in bacterial chemotaxis, *Proc. Natl. Acad. Sci. USA* **69**, 2509 (1972).
- [39] H. Szurmant and G. W. Ordal, Diversity in chemotaxis mechanisms among the bacteria and archaea, *Microbiol. Mol. Biol. Rev.* **68**, 301 (2004).
- [40] T. S. Shimizu, Y. Tu, and H. C. Berg, A modular gradient-sensing network for chemotaxis in *Escherichia coli* revealed by responses to time-varying stimuli, *Mol. Syst. Biol.* **6**, 382 (2010).
- [41] J. Long, S. W. Zucker, and T. Emonet, Feedback between motion and sensation provides non-linear boost in run-and-tumble navigation, *PLOS Comput. Biol.* **13**, e1005429 (2017).